

## Reaction Monitoring

International Edition: DOI: 10.1002/anie.201910052

German Edition: DOI: 10.1002/ange.201910052

# Rapid Chemical Reaction Monitoring by Digital Microfluidics-NMR: Proof of Principle Towards an Automated Synthetic Discovery Platform

Bing Wu, Sebastian von der Ecken, Ian Swyer, Chunliang Li, Amy Jenne, Franck Vincent, Daniel Schmidig, Till Kuehn, Armin Beck, Falko Busse, Henry Stronks, Ronald Soong, Aaron R. Wheeler,\* and André Simpson\*

**Abstract:** Microcoil nuclear magnetic resonance (NMR) has been interfaced with digital microfluidics (DMF) and is applied to monitor organic reactions in organic solvents as a proof of concept. DMF permits droplets to be moved and mixed inside the NMR spectrometer to initiate reactions while using sub-microliter volumes of reagent, opening up the potential to follow the reactions of scarce or expensive reagents. By setting up the spectrometer shims on a reagent droplet, data acquisition can be started immediately upon droplet mixing and is only limited by the rate at which NMR data can be collected, allowing the monitoring of fast reactions. Here we report a cyclohexene carbonate hydrolysis in dimethylformamide and a Knoevenagel condensation in methanol/water. This is to our knowledge the first time rapid organic reactions in organic solvents have been monitored by high field DMF-NMR. The study represents a key first step towards larger DMF-NMR arrays that could in future serve as discovery platforms, where computer controlled DMF automates mixing/titration of chemical libraries and NMR is used to study the structures formed and kinetics in real time.

Digital microfluidics is a powerful technique in which droplets are moved over an open array of electrodes.<sup>[1]</sup> The

approach permits a wide range of applications including proteomic sample preparation,<sup>[2]</sup> immunoassays,<sup>[3]</sup> organic synthesis,<sup>[4]</sup> and cell culture and analysis.<sup>[5]</sup> As such, interfacing with high field NMR, one of the most powerful analytical detectors for chemical structures<sup>[6]</sup> and interactions,<sup>[7]</sup> holds exciting promise. To date, two papers have been published on the interface of DMF and high field NMR. The first demonstrated the concept but was limited as the DMF device was placed on top of an existing NMR microcoil and the one-plate DMF device was limited to basic droplet movements.<sup>[8]</sup> The second paper introduced a two-plate DMF device that is much more versatile, with reagents dissolved in water aimed at biological applications.<sup>[9]</sup> However, DMF-NMR also holds great promise for organic chemistry research. For example, in digital microfluidics discrete droplets are moved and measured directly, the elimination of capillary dead volumes in connectors and tubing means the entire available volume can be placed over the NMR coil. In turn, this allows very small samples to be analyzed directly, important if expensive chemicals or precious samples need to be reacted and monitored. Furthermore, in the future it is possible to envision large DMF arrays<sup>[10]</sup> that have the potential to screen reactions from various combinations of substrates under automation. In many ways such an approach would turn DMF-NMR from an analytical tool into a discovery platform.

In this study two basic questions are asked: 1) As DMF-NMR has yet to be demonstrated with an organic reaction in an organic solvent, is this feasible? (i.e. can organic solvents, which have considerably less surface tension than water, be held and moved vertically (along the NMR magnet bore), against gravity, when sandwiched between the plates of a DMF device?) and 2) Can DMF-NMR be used to follow a rapid reaction (i.e. a reaction that completes faster than loading/match-tuning/shimming in conventional NMR (approximately 5 min) would allow)? To address these questions a simple hydrolysis of a cyclic carbonate in dimethylformamide is monitored, as-well as a Knoevenagel condensation in methanol/water. (Note as “digital microfluidics” and “dimethylformamide” have the same acronym, in this paper “DMF” is used for digital microfluidics while dimethylformamide is written in full.)

It is necessary to probe reaction kinetics in real-time to gain a thorough understanding of their mechanisms.<sup>[11]</sup> Traditionally, optical spectroscopies (e.g. UV-vis, IR, fluorescence, Raman spectroscopy) have been used to monitor chemical

[\*] Dr. B. Wu, A. Jenne, Dr. R. Soong, Prof. A. Simpson  
Department of Chemistry, University of Toronto Scarborough  
1265 Military Trail, Toronto, ON, M1C 1A4 (Canada)  
E-mail: andre.simpson@utoronto.ca

Dr. S. von der Ecken, Dr. I. Swyer, Prof. A. R. Wheeler  
Department of Chemistry, University of Toronto  
80 St. George St., Toronto, ON, M5S 3H6 (Canada)  
E-mail: aaron.wheeler@utoronto.ca

Dr. C. Li  
Laboratory of Physical Chemistry, Eindhoven University of Technology,  
P.O. Box 513, 5600 MB Eindhoven (The Netherlands)

Dr. F. Vincent, Dr. D. Schmidig, Dr. T. Kuehn, Dr. A. Beck  
Bruker BioSpin AG  
Industriestrasse 26, 8117 Fällanden (Switzerland)

Dr. F. Busse  
Bruker BioSpin GmbH  
Silberstreifen 4, 76287 Rheinstetten (Germany)

Dr. H. Stronks  
Bruker Canada Ltd.  
2800 High Point Drive, Milton, Ontario, L9T 6P4 (Canada)

Supporting information and the ORCID identification number(s) for the author(s) of this article can be found under <https://doi.org/10.1002/anie.201910052>.

reaction kinetics because of their widespread availability.<sup>[12]</sup> However, such approaches only offer limited chemical information compared to NMR.<sup>[13]</sup> Alternatively, mass spectrometry (MS) can be employed, but MS faces other challenges, including, the inability to distinguish between isomers.<sup>[14]</sup> The “Achilles’ heel” of NMR is its relatively low mass sensitivity. However, as the droplets used for DMF are generally quite small (i.e., pL to  $\mu$ L) NMR microcoils can be used to increase mass sensitivity. This approach leverages the fact that the magnetic flux density induced by a unit current (and therefore the voltage induced in the coil by nuclear spins) increases at a greater rate than the resistive noise, leading to improved signal-to-noise ratios. Despite the fact that planar microcoils are relatively well developed and give excellent NMR mass sensitivity,<sup>[15]</sup> they have not found routine application because of difficulties in sample handling for such small volumes of liquid. DMF solves the sample handling aspect, while the increased mass sensitivity of microcoils opens up the future potential for routine analysis of tiny samples.

The schematics in Figure 1 illustrate (a) the principle of digital microfluidics, (b) the NMR-DMF integration, and (c) the experimental protocol. The DMF-NMR assembly (Figure 1 b) is described in the supporting information and in our previous work.<sup>[9]</sup> Briefly, the top plate and bottom plate are assembled along with an electrical manifold and housing to connect to a standard MIC-5 imaging probe, and then loaded into an 11.7 T Bruker Avance III spectrometer. The plates are separated by 0.18 mm such that unit-droplets of reagents (covering one actuation electrode) were approximately 911 nL and the volume of sample within the field lines of the microcoil (0.98 mm OD) was approximately 136 nL. As previously demonstrated,<sup>[9]</sup> during NMR acquisition the droplets are actively stretched along the  $B_0$  direction (direction of the external magnetic field) to produce an elongated shape that is more amenable to shimming using the vertically orientated shims on standard NMR spectrometers. Shimming can be performed on either a dummy reaction as previously described<sup>[9]</sup> or by shimming on one of the reactant droplets; the latter was used for the data reported here. Before the probe is inserted into the NMR system different chemical reagents are loaded on the bottom-plate in separate droplets (Figure 1-c.1). Figure 1-c.2 shows how the two droplets (orange, blue) are moved on the device, while being inside the NMR system. The pre-shimming is also performed on the first droplet (blue) at this stage. After the shimming is complete the reactants are merged, mixed (Figure 1-c.3) and brought over the microcoil to monitor the reaction (Figure 1-c.4). The DMF device is controlled using an open-source Droplet control-system.<sup>[16]</sup> The voltage for droplet actuation was set to 145–165  $V_{\text{rms}}$  at 10 kHz.

A model reaction was used to test the capability of the DMF-NMR system for carrying out organic reactions in organic solvents. A hydrolysis reaction in dimethylformamide was selected, in part because optically active diols are important intermediates for synthesizing natural products as well as biologically active compounds.<sup>[17]</sup> Scheme 1 shows the cyclohexene carbonate hydrolysis reaction<sup>[18]</sup> studied here. To increase the reaction rate, triazabicyclodecene (TBD) was

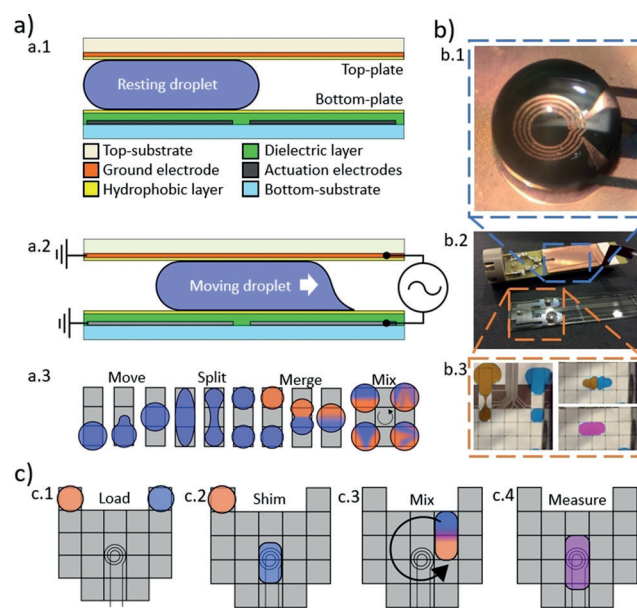
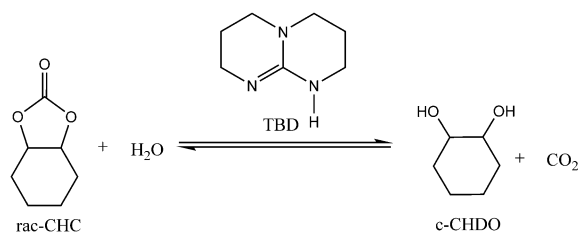


**Figure 1.** Functional principle of digital microfluidics (DMF) and its integration with NMR. (a.1) Schematic side-view of a DMF device. The bottom-plate features an array of actuation electrodes (chromium, grey) on a bottom-substrate (glass, light blue), which are covered by a dielectric layer (Parylene, green) and a hydrophobic coating (Fluoropel, yellow). The top-plate features a ground electrode (copper, orange), and a hydrophobic layer (Fluoropel, yellow). (a.2) Schematic side-view, illustrating how a force can be induced on the droplet by applying a voltage between an actuation and a ground electrode. (a.3) Schematic top-views, illustrating how activating the electrodes in specific patterns allows the basic fluid operations: moving, splitting/dispersing, merging, and mixing. (b) Photographs of NMR coil and DMF top-plate. (b.1) A 500  $\mu\text{m}$  (I.D.) 980  $\mu\text{m}$  (O.D.) planar microcoil is integrated into the ground electrode on the top-substrate, which is mounted on a holder. (b.2) The holder (top) functions as the top-plate, and the DMF bottom-plate (bottom) comprises the actuation electrode array. A detailed description of the hardware setup can be found in our previous work.<sup>[9]</sup> (b.3) Frames from a video of a DMF experiment in which two droplets are dispensed from reservoirs and then merged and mixed on the array of electrodes. Artificial colour has been added to the droplets to aid in visualization. (c) Schematic top-view of the positioning of actuation electrode array of the bottom-plate, the NMR coil of the top-plate, and the droplets sandwiched in between. (c.1) Reactants are loaded into the device. (c.2) Reactant “blue” is moved over the coil for shimming and moved back to its starting position. This is repeated with reactant “orange”. (c.3) Both reactants are mixed and moved into the detection site over the coil. (c.4) The previously acquired shims are used for measurement permitting acquisition to be started immediately. Note that for clarity in (c.3) the droplets are shown to be mixed in a large circle but in practice they are mixed over the NMR coil to permit NMR data to be acquired during the mixing process.

employed as a strong nucleophilic catalyst and to create the basic condition required for rapid conversion.<sup>[19]</sup>

The model reaction studied here has rapid kinetics, and thus following its progress is out of reach for conventional NMR systems. Specifically, loading, matching/tuning and automated shimming protocols take many minutes, such that reactions like the one in Scheme 1 can proceed to completion prior to the first measurement. With DMF-NMR, reagents can be injected and reacted without moving the



**Scheme 1.** TBD-catalyzed hydrolysis of racemic cyclohexene carbonate (*rac*-CHC) to *cis*-1,2-cyclohexanediol (*c*-CHDO).

reaction vessel, such that the matching and tuning remains constant throughout the process. After pre-shimming, on initialization of the reaction (including a 10 s mixing step in which the merged droplet is manipulated across the array, Figure 1-c.3–4), data can be collected without delay. In typical experiments, spectra were collected every 5 seconds, providing sufficient temporal resolution to follow the progress of the reaction evaluated here. This sampling frequency is much faster than that reported in previous DMF-NMR analyses.<sup>[8,9]</sup> In theory, in future applications with ultrafast reactions (sensitivity permitting) it should be possible to collect NMR data in even shorter time frames; for example, collection of even full 2D datasets have been reported in as little as 100 ms using cutting edge ultrafast 2D NMR.<sup>[20]</sup> In such applications the mixing on chip and pre-shimming are key steps which permit NMR data collection to start at exactly the same time as the reaction is initiated. For example, a recent pioneering study that developed tapered stripline NMR coils to follow rapid reactions in a capillary, cited that the rapid mixing of the reagents in a narrow capillary was the limiting factor rather than the NMR detection itself.<sup>[21]</sup>

Figure 2 shows the <sup>1</sup>H DMF-NMR data for the model hydrolysis reaction and corresponding concentration plots. First, it is important to note here that data are plotted from 15 seconds onwards. In the first 10 seconds the reactants are being actively mixed, after which the droplet is allowed to stabilize for 5 seconds. As such during this time the integrals are less stable as the droplet content is changing dynamically, making it challenging to extract kinetic data. However, it is still possible to collect NMR data during this initial window (see Figure S2) which would be important to monitor rapid qualitative changes (i.e. new products formed, intermediates formed) as soon as the droplets are brought together. After the first 15 seconds the data show a steady consumption of starting material *rac*-CHC (green and blue), with a corresponding increase in concentration of product *cis*-1,2-cyclohexanediol (*c*-CHDO) (red) (detailed NMR spectral assignments are shown in Figure S3–S7, including diffusion ordered spectroscopy (DOSY) which is a powerful tool for separating products and studying non-covalent interactions). Note that water ([H<sub>2</sub>O] = 8 M) was included in the CHC reagent droplet to accelerate the reaction and to suppress the cyclic ring polymerization on mixing with TBD,<sup>[19,22]</sup> although a trace amount of polymer still formed (Figure S5). Likewise, a reference standard, isopropyl alcohol (IPA), was included in the TBD reagent droplet to permit normalization between runs and to correct for changes not caused by the reaction.

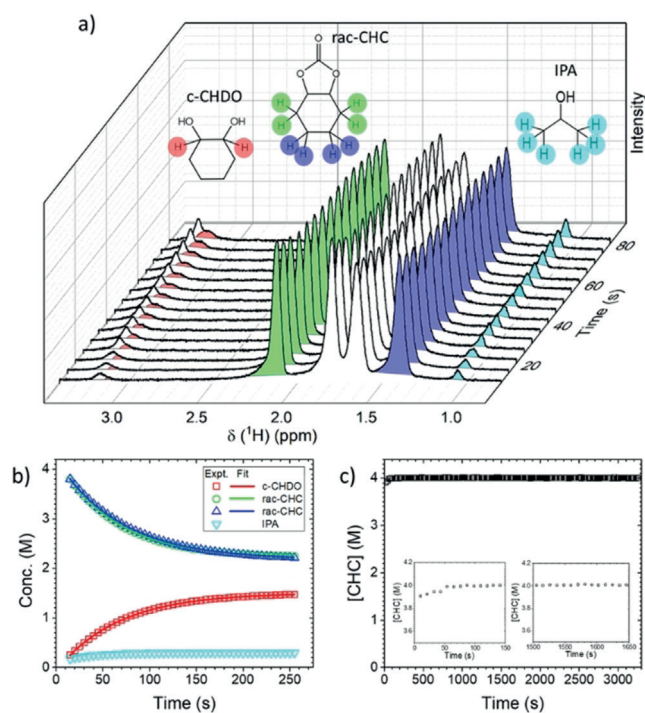


**Figure 2.** DMF-NMR for fast reaction analysis. (a) Representative spectra collected during the *rac*-CHC hydrolysis reaction ([*rac*-CHC] = 4 M) to *c*-CHDO in [D<sub>7</sub>]DMF, with peaks highlighted that represent CHC protons (green, blue), *c*-CHDO protons (red), and IPA protons (turquoise). (b) Concentrations as a function of time extrapolated from peaks correlated to *rac*-CHC (blue triangles and green circles), *c*-CHDO (red squares), IPA (turquoise triangles) (see the detailed chemical shift assignments in SI). (c) Concentrations as a function of time for pure *rac*-CHC (4 M). Insets are magnified regions at the beginning (left) and in the middle (right) of the experiment.

Concentrations as a function of time were calculated for all species. As shown in Figure 2b, the internal standard (IPA) signal appears to increase for the first minute of the analysis, after which it plateaus. We hypothesize that this may reflect a subtle droplet shape change that takes effect in the first minute of incubation above the coil. Another potential explanation is that it is related to evaporation of solvent. To investigate this effect further, a control study was carried out in which droplets of reagent (*rac*-CHC dimethylformamide-*d*<sub>7</sub> solution) and solvent (pure dimethylformamide-*d*<sub>7</sub>) were treated as above, and then analyzed for a longer period of time (Figure 2c). As shown, there is (again) a small signal increase observed in the first minute, with negligible changes observed for the remainder of the experiment (> 50 min). The signal stability over this long duration suggests that evaporation is not causing appreciable changes to the signal. More work is needed to explore, but regardless of the mechanism, the inclusion of the internal standard allowed for reactant and product integrals to be corrected to obtain precise kinetic parameters.

The corrected reagent and product concentration data for the model hydrolysis reaction (Figure 2b) exhibit exponential behaviour with time that is consistent with simple 1st order reaction kinetics. As outlined previously,<sup>[23]</sup> TBD is a basic catalyst that acts as a proton bridge because of the synergistic

action of its two N atoms. Therefore, the promotion of proton transfer results in a base-catalyzed reaction that follows pseudo-first order reaction kinetics.<sup>[24]</sup> As shown in Figure 3, this was tested in the DMF-NMR system for different

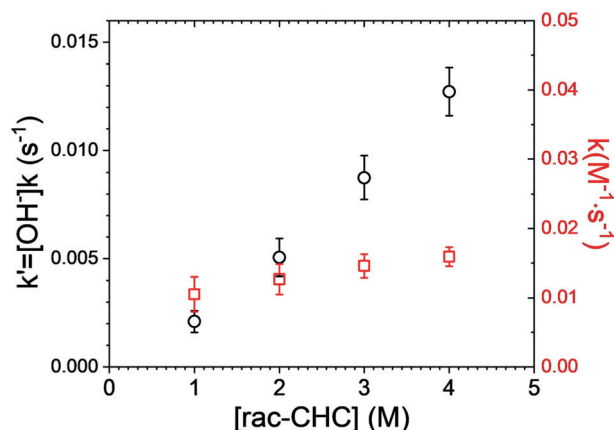


**Figure 3.** DMF-NMR hydrolysis reaction kinetics. Plot of the pseudo-first order reaction constant  $k'$  (black circles, left axis), and the second order reaction constant  $k$  (red boxes, right axis) as a function of the concentration of reactant *rac*-CHC. (The ratio between reactant and catalyst concentration in all the cases was held at 10:1). Error bars represent  $\pm$  standard deviation for  $n=6$ .

concentrations of reagent, while maintaining a constant ratio of reagent:catalyst. For example, the calculated reaction rate constant is  $k' = 0.0127 \pm 0.0011 \text{ s}^{-1}$  for initial *rac*-CHC concentration = 4 M, which is similar to what was reported from alkaline hydrolysis of cyclic carbonate using a conventional instrument.<sup>[25]</sup> This indicates that at sub- $\mu\text{L}$  volumes, the reaction follows the same chemical kinetics observed with larger volumes. As reported previously,<sup>[26]</sup> the second-order rate constant  $k$  for base-catalyzed reactions can be obtained by dividing  $k'$  by base concentration. Using [TBD] as an approximation,  $k$  was calculated here to be around  $0.014 \pm 0.002 \text{ M}^{-1} \text{ s}^{-1}$  for *rac*-CHC, again consistent with previous reports.<sup>[26a]</sup> In summary, Figure 3 demonstrates that DMF-NMR can be used to explore features of chemical reactions while only consuming small volumes of reagents.

Finally, a reaction in a methanol/water solvent was evaluated to test the performance of the DMF-NMR system with volatile constituents. The Knoevenagel condensation and Michael addition between dimedone (DIM) and benzoic acid (BA) to form tetraketones (TKs)<sup>[27]</sup> (Scheme S1) was selected as a model system for this test, in recognition of the role of TKs as key intermediates for synthesizing heterocycles. Figure 4a and 4b show NMR data and associated kinetics for the model reaction, with assignments provided in the supporting materials (Figures S8–S9). We expected that evaporation might be more significant in this system (with a volatile solvent) than the one described above; thus, an internal standard, tetramethylsilane (TMS) was used and its signal was evaluated as a function of time (Figure 4c). As shown, in 25 min the internal standard concentration increases by  $\approx 10\%$ , suggesting that a similar amount of solvent evaporates during the reaction. In the future (if

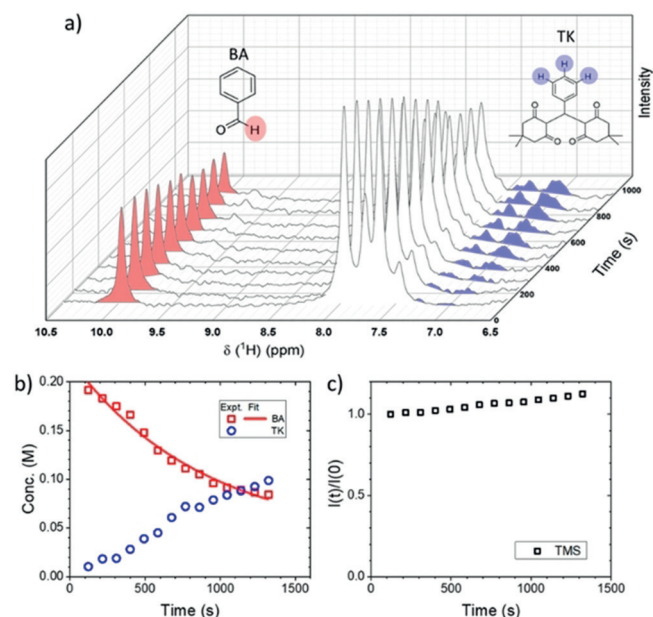


**Figure 4.** DMF-NMR for analysis of reactions in volatile solvents. (a) Representative spectra collected during the Knoevenagel condensation and Michael addition of BA ([BA]=0.1 M) to form TKs, with peaks highlighted that represent BA protons (red) and TK protons (blue). (b) Concentrations as a function of time extrapolated from peaks BA (red squares) and TK (blue circles). (Detailed chemical shift assignment in Figure S8–9.) (c) The integrated peak area as a function of time  $I(t)$  relative to the initial integrated peak area  $I(0)$  for the peak corresponding to the internal standard TMS.

needed), this effect might be diminished by sealing the device. For the purposes described here, however, it was sufficient to simply correct the data shown in Figure 4b for evaporation effects, allowing calculation of the reaction rate constant of  $0.0011 \text{ s}^{-1}$ , based on a first order reaction mechanism proposed by previous studies.<sup>[28]</sup> To our knowledge, this is the first reaction rate constant reported for this reaction.

In conclusion, this communication demonstrates a unique application of DMF-NMR: fast reaction monitoring of organic reactions in organic solvents. By pre-shimming on a reactant droplet, the reaction can be monitored immediately on mixing allowing reactions with rapid kinetics to be monitored. The small volumes inherent to DMF allow the use of tiny amounts of reagents. For example, in the tandem Knoevenagel condensation and Michael addition, a unit-droplet covering a single electrode (911 nL) would contain only 6.3  $\mu\text{g}$  of DIM and 9.4  $\mu\text{g}$  of BA, and the active volume above the coil (136 nL) would contain only 0.94  $\mu\text{g}$  and 1.4  $\mu\text{g}$ , respectively. As such this opens up the possibility of studying various reaction conditions using NMR, even with limited or precious reagents. Here the DMF-NMR measured reaction rate constants that are consistent with literature values indicating the rate determined at  $\mu\text{L}$ -volume, still follows the expected chemical kinetics observed with larger volumes.

In future, the possibility of using larger DMF chips could provide the space for multiple reagents and solvent reservoirs. As mixing and movement of the reagents is fully computer

controlled and automated, this opens up the potential for DMF with NMR detection as a synthetic “discovery tool”, where a range of conditions could be screened to either characterize a known reaction in detail or search for novel reactions and unexpected products while using only tiny amounts of reagents. Given that DMF can automate sample-handling and reactions and NMR provides unparalleled de novo structure elucidation, it is more a question of *when* DMF-NMR will become an everyday tool in organic chemistry research rather than *if*.

### Acknowledgements

We thank the National Science and Engineering Research Council (NSERC) (STPGP 494273-16), the Canada Foundation for Innovation (CFI), the Ontario Ministry of Research and Innovation (MRI), and the Krembil Foundation for providing funding. A.S. thanks the Government of Ontario for an Early Researcher Award. A.R.W. thanks the Canada Research Chairs (CRC) Association for a CRC.

### Conflict of interest

The authors declare no conflict of interest.

**Keywords:** digital microfluidics · hydrolysis · NMR spectroscopy · rapid reactions · reaction monitoring

**How to cite:** *Angew. Chem. Int. Ed.* **2019**, *58*, 15372–15376  
*Angew. Chem.* **2019**, *131*, 15516–15520

- [1] a) J. Berthier, *Micro-drops and digital microfluidics*, 2nd ed., Elsevier/WA, Amsterdam, **2013**; b) K. Choi, A. H. C. Ng, R. Fobel, A. R. Wheeler, *Annu. Rev. Anal. Chem.* **2012**, *5*, 413–440.
- [2] a) H. Moon, A. R. Wheeler, R. L. Garrell, J. A. Loo, C. J. Kim, *Lab Chip* **2006**, *6*, 1213–1219; b) V. N. Luk, A. R. Wheeler, *Anal. Chem.* **2009**, *81*, 4524–4530.
- [3] a) K. Choi, A. H. C. Ng, R. Fobel, D. A. Chang-Yen, L. E. Yarnell, E. L. Pearson, C. M. Oleksak, A. T. Fischer, R. P. Luoma, J. M. Robinson, J. Audet, A. R. Wheeler, *Anal. Chem.* **2013**, *85*, 9638–9646; b) L. Coudron, M. B. McDonnell, I. Munro, D. K. McCluskey, I. D. Johnston, C. K. L. Tan, M. C. Tracey, *Biosens. Bioelectron.* **2019**, *128*, 52–60.
- [4] a) M. J. Jebrail, A. H. C. Ng, V. Rai, R. Hili, A. K. Yudin, A. R. Wheeler, *Angew. Chem. Int. Ed.* **2010**, *49*, 8625–8629; *Angew. Chem.* **2010**, *122*, 8807–8811; b) P. Y. Keng, S. P. Chen, H. J. Ding, S. Sadeghi, G. J. Shah, A. Dooraghi, M. E. Phelps, N. Satyamurthy, A. F. Chatziioannou, C. J. Kim, R. M. van Dam, P. Asgari, U. S. Dakarapu, J. Jeon, H. Moon, *Lab Chip* **2019**, *19*, 3054–3064.
- [5] a) A. H. C. Ng, M. D. Chamberlain, H. Situ, V. Lee, A. R. Wheeler, *Nat. Commun.* **2015**, *6*, 7513; b) M. Y. Chiang, Y. W. Hsu, H. Y. Hsieh, S. Y. Chen, S. K. Fan, *Sci. Adv.* **2016**, *2*, e1600964.
- [6] J. Fiaux, E. B. Bertelsen, A. L. Horwich, K. Wuthrich, *Nature* **2002**, *418*, 207–211.
- [7] C. L. Perrin, T. J. Dwyer, *Chem. Rev.* **1990**, *90*, 935–967.
- [8] I. Swyer, R. Soong, M. D. M. Dryden, M. Fey, W. E. Maas, A. Simpson, A. R. Wheeler, *Lab Chip* **2016**, *16*, 4424–4435.
- [9] I. Swyer, S. von der Ecken, B. Wu, A. Jenne, R. Soong, F. Vincent, D. Schmidig, T. Frei, F. Busse, H. J. Stronks, A. J. Simpson, A. R. Wheeler, *Lab Chip* **2019**, *19*, 641–653.
- [10] B. Hadwen, G. R. Broder, D. Morganti, A. Jacobs, C. Brown, J. R. Hector, Y. Kubota, H. Morgan, *Lab Chip* **2012**, *12*, 3305–3313.
- [11] a) R. G. Bergstrom, M. J. Cashen, Y. Chiang, A. J. Kresge, *J. Org. Chem.* **1979**, *44*, 1639–1642; b) J. Kerovuo, J. Rouvinen, F. Hatzack, *Biochem. J.* **2000**, *352*, 623–628.
- [12] a) R. F. Storey, A. B. Donnalley, T. L. Maggio, *Macromolecules* **1998**, *31*, 1523–1526; b) D. Gracin, V. Strukil, T. Friscic, I. Halasz, K. Uzarevic, *Angew. Chem. Int. Ed.* **2014**, *53*, 6193–6197; *Angew. Chem.* **2014**, *126*, 6307–6311.
- [13] G. L. Closs, R. J. Miller, *J. Am. Chem. Soc.* **1981**, *103*, 3586–3588.
- [14] C. A. Müller, A. Pfaltz, *Angew. Chem. Int. Ed.* **2008**, *47*, 3363–3366; *Angew. Chem.* **2008**, *120*, 3411–3414.
- [15] a) C. Massin, F. Vincent, A. Homsy, K. Ehrmann, G. Boero, P. A. Besse, A. Daridon, E. Verpoorte, N. F. de Rooij, R. S. Popovic, *J. Magn. Reson.* **2003**, *164*, 242–255; b) I. Fugarieu, R. Soong, D. Lane, M. Fey, W. Maas, F. Vincent, A. Beck, D. Schmidig, B. Treanor, A. J. Simpson, *Analyst* **2017**, *142*, 4812–4824.
- [16] R. Fobel, C. Fobel, A. R. Wheeler, *Appl. Phys. Lett.* **2013**, *102*.
- [17] a) A. B. Holmes, A. B. Tabor, R. Baker, *J. Chem. Soc. Perkin Trans. 1* **1991**, 3301–3306; b) T. L. Underiner, L. A. Paquette, *J. Org. Chem.* **1992**, *57*, 5438–5447.
- [18] M. Shimojo, K. Matsumoto, M. Hatanaka, *Tetrahedron* **2000**, *56*, 9281–9288.
- [19] M. Metzger, B. Strehle, S. Solchenbach, H. A. Gasteiger, *J. Electrochem. Soc.* **2016**, *163*, A1219–A1225.
- [20] P. Giraudeau, L. Frydman, *Annu. Rev. Anal. Chem.* **2014**, *7*, 129–161.
- [21] K. C. H. Tijssen, J. Bart, R. M. Tiggelaar, J. W. G. Janssen, A. P. M. Kentgens, P. J. M. van Bentum, *J. Magn. Reson.* **2016**, *263*, 136–146.
- [22] B. Ochiai, Y. Satoh, T. Endo, *Green Chem.* **2005**, *7*, 765–767.
- [23] J. Ma, X. L. Zhang, N. Zhao, F. K. Xiao, W. Wei, Y. H. Sun, *J. Mol. Struct. THEOCHEM* **2009**, *911*, 40–45.
- [24] J. F. Kirsch, W. P. Jencks, *J. Am. Chem. Soc.* **1964**, *86*, 833.
- [25] a) A. H. Saadi, W. H. Lee, *J. Chem. Soc. B* **1966**, 1–4; b) A. H. Saadi, W. H. Lee, *J. Chem. Soc. B* **1966**, 5–6.
- [26] a) E. T. Kaiser, M. Panar, F. H. Westheimer, *J. Am. Chem. Soc.* **1963**, *85*, 602–607; b) T. C. Bruice, S. J. Benkovic, *J. Am. Chem. Soc.* **1964**, *86*, 418–426.
- [27] J. J. Yu, L. M. Wang, J. Q. Liu, F. L. Guo, Y. Liu, N. Jiao, *Green Chem.* **2010**, *12*, 216–219.
- [28] C. P. Haas, U. Tallarek, *ChemistryOpen* **2019**, *8*, 606–614.

Manuscript received: August 7, 2019

Accepted manuscript online: August 26, 2019

Version of record online: September 12, 2019